Multicolor Spectral Karyotyping of Human Chromosomes

E. Schröck, S. du Manoir, T. Veldman, B. Schoell, J. Wienberg, M. A. Ferguson-Smith, Y. Ning, D. H. Ledbetter, I. Bar-Am, D. Soenksen, Y. Garini, T. Ried*

The simultaneous and unequivocal discernment of all human chromosomes in different colors would be of significant clinical and biologic importance. Whole-genome scanning by spectral karyotyping allowed instantaneous visualization of defined emission spectra for each human chromosome after fluorescence in situ hybridization. By means of computer separation (classification) of spectra, spectrally overlapping chromosome-specific DNA probes could be resolved, and all human chromosomes were simultaneously identified.

Cytogenetic analysis of numerical and structural chromosomal aberrations in pre- and postnatal diagnostics and cancer cytogenetics is an integral part of clinical care (*1*). Fluorescence in situ hybridization (FISH) has been used as an adjunct to routine cytogenetics to achieve a higher sensitivity, specificity, and resolution of chromosome aberrations than is possible by banding analysis (karyotyping). The diagnostic potential of FISH would be greatly improved by the ability to analyze the entire genome simultaneously on the basis of the differential display of all human chromosomes. However, the limited number of spectrally nonoverlapping fluorochromes has prevented the use of FISH to simultaneously discriminate all human chromosomes in different colors in the diagnostic laboratory.

Here, we report the development of a spectral imaging approach that combines Fourier spectroscopy, charge-coupled device (CCD) imaging, and optical microscopy to measure simultaneously at all points in the sample emission spectra in the visible and near-infrared spectral range (Fig. 1). This allows the use of multiple spectrally overlapping probes (*2*). The approach is based on the measurement of a discrete spectrum (identified from a sequence of intensities at every pixel measured at many different wavelengths), which facilitates the discrimination of multiple fluorophores. In contrast to conventional epifluorescence microscopy in which fluorochrome discrimination is based on the measurement of a single intensity through a fluorochrome-specific optical filter (*3*), the use of spectral karyotyping allows all information within the spectrum of emitted light to be used for analysis.

The principle of spectral imaging and spectra-specific chromosome classification is illustrated in Fig. 1. The emission spectra of differentially labeled chromosome painting probes specific for chromosome 7 (labeled with Cy3), chromosome 13 (labeled with Texas Red), and chromosome 4 (labeled with both Cy3 and Texas Red) were measured in one exposure through a custom triple bandpass filter. The Sagnac interferometer in the optical head of the spectral cube creates an optical path difference of the light emitted from the chromosome painting probes. The subtle differences in the emission spectra of these fluorophores after passage through the interferometer are sufficient to enable spectrum-specific image capture with a CCD camera. The conversion of emission spectra to the visualization of display colors is achieved by assigning blue, green, and red colors to specific spectral ranges. The display colors allow the assessment of the quality of the hybridization (for example, uniformity of hybridization and signal brightness) and are used as a first evaluation of the hybridization directly after image acquisition and without further computation. The display colors are therefore similar for spectrally overlapping fluorochromes because the color discrimination is similar to that achieved by conventional epifluorescence microscopy (Fig. 1, display colors inset). In contrast, the classification of chromosomes after Fourier transformation and assignment of a classification color is based on the spectrum that has been measured at every given pixel. The algorithms used for spectral classification (*6*) produce an image in which the same classification color is assigned to all pixels with the same spectrum (Fig. 1, classification colors inset). For the example shown in Fig. 1, fluorophores with overlapping emission spectra were purposely selected to illustrate the value of assigning spectral-based classification colors that can be readily discerned.

The spectral-based method for discriminating the spectrally overlapping fluorophores (classification) shown in Fig. 1 is readily extended to a much larger number of fluorochromes, provided there are measurable differences (estimated currently at $\geq$15 nm) in the emission spectrum of each fluorochrome. We applied this method of spectral imaging of FISH experiments as a genome scanning method to simultaneously identify each human chromosome in metaphase preparations, an approach we refer to as spectral karyotyping. Chromosome-specific composite libraries generated by polymerase chain reaction from flow-sorted human chromosomes were directly labeled with nucleotides conjugated to five different fluorophores (Cy2, Spectrum Green, Cy3, Texas Red, and Cy5) or combinations thereof (*4*). A composite probe set containing all 24 chromosomes was hybridized to normal metaphase chromosomes (Fig. 2). Chromosome-specific labeling is achieved by suppression hybridization. Specifically, repetitive sequences in the composite libraries are blocked by the addition of an excess of unlabeled human DNA enriched for repetitive sequences (Cot-1 DNA). This suppression of repetitive sequences is illustrated for chromosome 1 (where the paracentromeric heterochromatin of chromosome 1 is not labeled), and for the acrocentric chromosomes 13 through 15, 21, and 22 (where the ribosomal cistrons on the terminal p arm are assigned a different color from the chromosome-specific DNA). As in any other FISH experiment that uses suppression hybridization, these regions are excluded from analysis. The hybridization is presented in both display (Fig. 2A) and classification colors (Fig. 2, B and C). Display colors allow all human chromosomes to be readily visualized after spectral imaging (*5*), and on the basis of spectral measurements at each pixel, a chromosome classification algorithm was applied to spectrally karyotype all human chromosomes (Fig. 2C) (*6*).

We explored the potential of spectral karyotyping as a screening method for chromosomal aberrations by analyzing clinical samples from multiple laboratories where conventional banding methods or FISH with chromosome painting probes had been previously performed (Fig. 3). Spectral karyotyping was performed without prior knowledge of the chromosomal aberrations. In all cases Giemsa banding (G-banding) and spectral karyotyping revealed consistent results. In some cases, G-banding was not sufficient to entirely interpret the chromosomal aberrations. In these cases, the diagnosis of chromosomal aberrations by spectral karyotyping was confirmed

E. Schröck, S. du Manoir, T. Veldman, B. Schoell, Y. Ning, D. H. Ledbetter, T. Ried, Diagnostic Development Branch, National Center for Human Genome Research, National Institutes of Health, 49 Convent Drive, Building 49, Room 4A28, Bethesda, MD 20892–4470, USA.
J. Wienberg and M. A. Ferguson-Smith, Department of Pathology, Cambridge University, Cambridge CB21QP, UK.
I. Bar-Am, Department of Cell Research and Immunology, Tel-Aviv University, Tel Aviv 69978, Israel.
D. Soenksen, Applied Spectral Imaging, Incorporated, Carlsbad, CA 92009, USA.
Y. Garini, Applied Spectral Imaging, Limited, Migdal Haemek, 10551 Israel.

*To whom correspondence should be addressed. E-mail: tried@nchgr.nih.gov

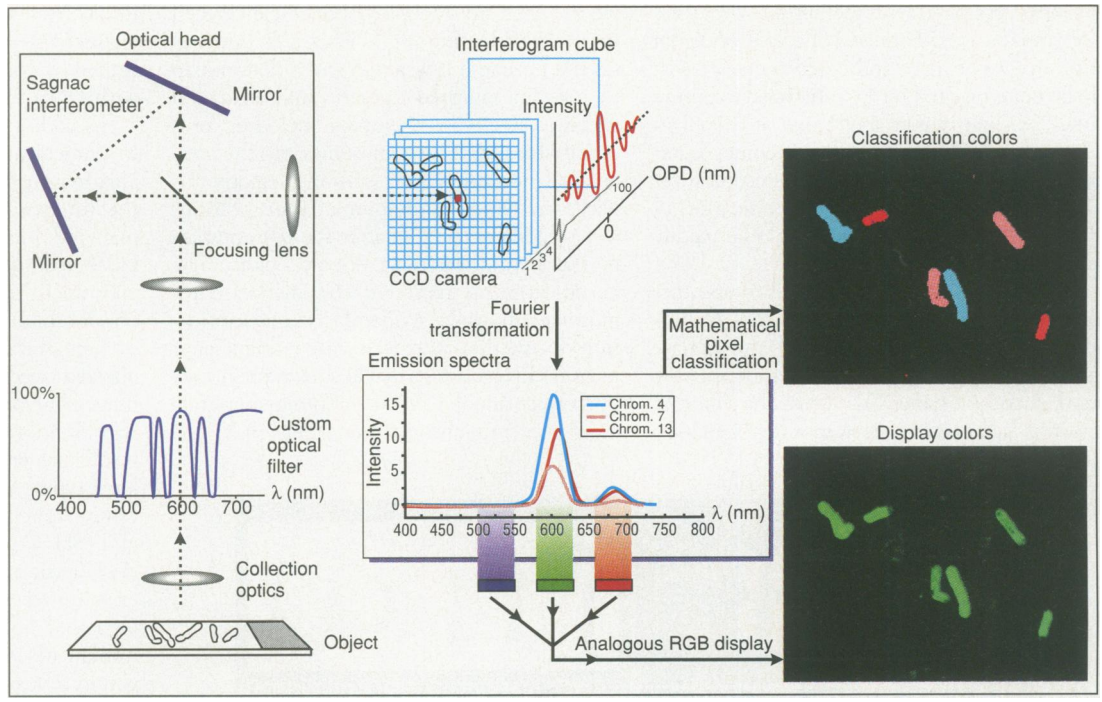

Fig. 1. Principle of spectral imaging and demonstration of the potential of separating overlapping fluorochromes with spectra-based classification. Simultaneous hybridization of three different chromosome painting probes that were labeled with Cy3 (chromosome 7), Texas Red (chromosome 13), and a combination of Cy3 and Texas Red (chromosome 4) is depicted. The emitted light is visualized through a triple bandpass filter, sent through an interferometer, and imaged with a CCD camera. The interferogram that is generated for each pixel is analyzed by Fourier transformation, a process that makes it possible to define the spectrum of the light (*5*). The measured spectra can then be converted to display colors or to classification colors (*6*). When display colors are used, chromosomes with similar spectra have similar colors. However, the subtle differences in the spectra of the Cy3- and Texas Red–labeled chromosome painting probes are sufficient to enable the discrimination of the chromosomes after spectral classification. OPD, optical path difference.

with conventional dual color FISH analysis. The smallest discernible aberration analyzed for this report was a translocation t(1;11)(q44;p15.3) in which the reciprocal translocation was unrecognizable by conventional banding analysis. The origin of the chromosomal material that contributed to the reciprocal translocation was correctly classified (Fig. 3A). The translocated segments on chromosomes 1 and 11 were confirmed by subtelomere-specific cosmid probes for chromosomes 1q and 11p (*7*). On the basis of the location of the probes used, the size of the alteration was estimated to be >1500 kbp. In a second case, banding analysis suggested a translocation of a segment of chromosome 4 to chromosome 12. Spectral karyotyping unambiguously identified and classified the origin of the additional chromosomal material as being derived from chromosome 4 (Fig. 3B). Other examples include the identification by spectral karyotyping of a translocation t(8;13)(q24.1;q34) and the recognition of the 47,XXY karyotype of a Klinefelter syndrome patient (*8*).

We assessed classification variations from one metaphase to another of a single hybridization by analyzing the chromosomes of five randomly selected metaphases from all cases. In all instances, the marker chromosomes could be consistently visualized and characterized after spectral classification. For example, the chromosome translocations detected in the cases presented in Fig. 3, A and B, were observed in all metaphases analyzed. To determine the limit of sensitivity of spectral karyotyping, we examined a case with a submicroscopic translocation (unrecognizable in both metaphase and prometaphase chromosomes) involving chromosomes 16 and 17. This t(16;17) had been previously demonstrated by FISH with cosmid probes, and the reciprocal interchange of chromatin was estimated at ~500 kbp. Spectral karyotyping with metaphase chromosomes from this patient failed to identify the known t(16;17), suggesting that the limit of sensitivity for metaphase chromosome analysis with currently available painting probes is between 500 and 1500 kbp.

To demonstrate that spectral karyotyping is an approach that can be used to complement conventional banding analysis, we repeated the hybridization on previously G-banded chromosomes. Probably because of the trypsin digestion that is required for G-banding, the signal intensity was slightly re-

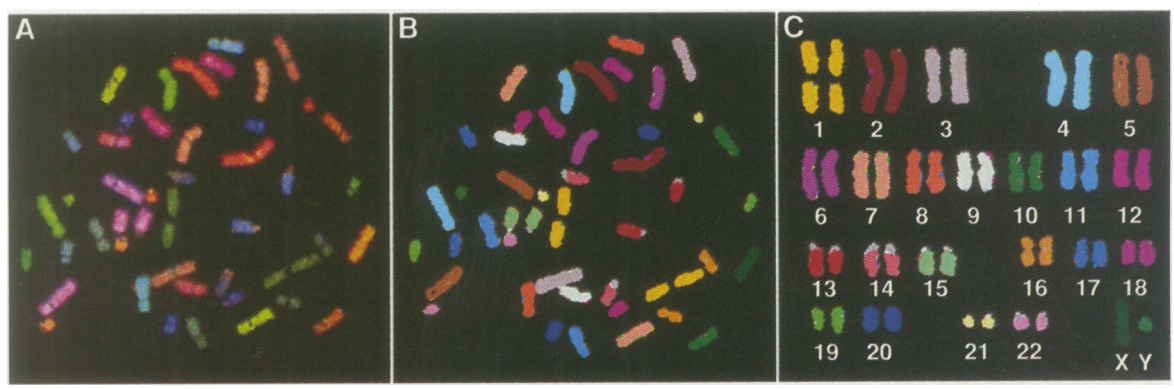

Fig. 2. Spectral karyotyping of human chromosomes after the simultaneous hybridization of 24 combinatorially labeled chromosome painting probes. (**A**) Presentation of display colors. (**B**) Presentation of spectra-based classification colors. Regions rich in repetitive sequences, for example, the short arms of chromosomes 13, 14, 15, 21, and 22, show color variations that are expected after suppression hybridization. (**C**) Karyotype of the classification-colored metaphase chromosomes shown in (B).

duced as compared with metaphases that were not previously G-banded. The loss of signal intensity was ~10% and could therefore easily be compensated for by prolonged exposure times. A slightly increased noise at the edges of previously G-banded chromosomes compared with non–G-banded chromosomes was also observed. However, the classification of the metaphase chromosomes could be readily achieved (Fig. 2).

The cytogenetic analysis of chromosomes from tumor cells is often hampered by low mitotic indices, poor quality metaphase spreads, and the presence of unidentifiable marker chromosomes. To assess the value of spectral karyotyping in tumor cytogenetics, we analyzed an aneuploid breast cancer cell line (SKBR3) (Fig. 3C). This cell line was selected because it was previously determined to contain multiple numeric and structural chromosome rearrangements including unidentifiable marker chromosomes and the presence of homogeneously staining regions. Indeed, numerous chromosomal translocations were readily detectable after the presentation of the hybridization in display colors. The classification of representative marker chromosomes allowed the unambiguous identification of structural alterations including a giant marker chromosome (mar1) shown previously by conventional FISH to contain amplified sequences from chromosome 8 (Fig. 3C). The results from spectral karyotyping indicative of an increased copy number for 8q were confirmed by comparative genomic hybridization with DNA extracted from this cell line (9).

In addition to the diagnostic applications in clinical and cancer cytogenetics, spectral karyotyping should be of considerable value in the interspecies study (such as between human and primates) of evolutionary divergence by comparative cytogenetics. For example, in contrast to the current practice of analysis of chromosome morphology sequentially for all 24 human chromosomes, spectral karyotyping allowed reconstruction of the highly rearranged karyotype of a gibbon species after one hybridization (Fig. 3, D and E). Although our results are preliminary, the results of spectral karyotyping are in excellent agreement with results from previously performed conventional FISH experiments and banding analysis (*10*). Basic research applications can also be envisioned to include the analysis of chromosomal aberrations in animal models of human diseases and in work under way to generate a multicolor banding pattern (bar code) of the human chromosome complement by using a combination of chromosome arm– and chromosome band–specific painting probes that will also allow visualization of intrachromosomal rearrangements (*11*). This study suggests that spectral karyotyping could be an important tool for rapid and automatic karyotyping, as well as for facilitating the identification of chromosome abnormalities in humans.

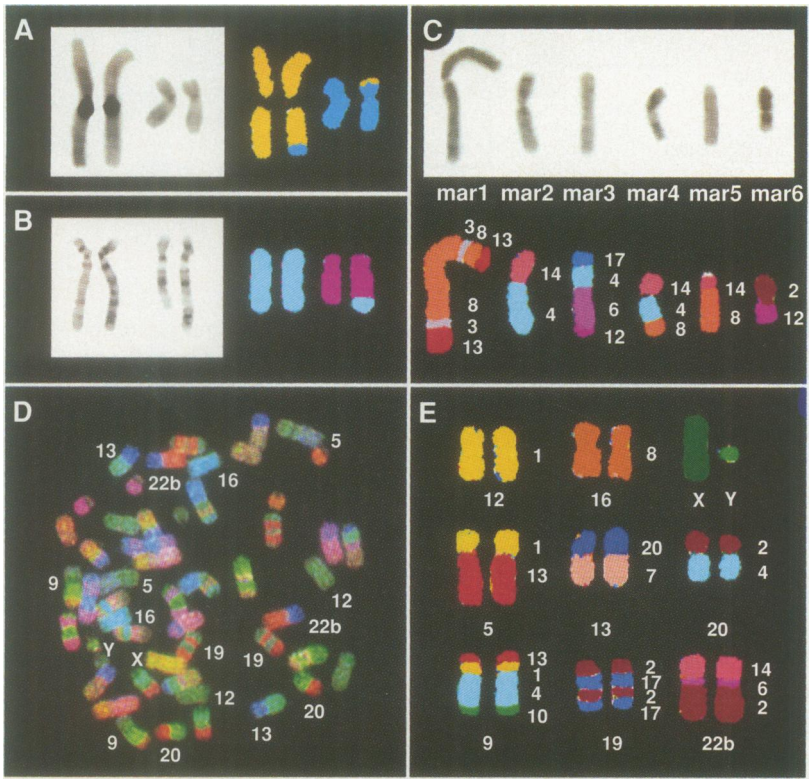

Fig. 3. (**A**) Example of spectral karyotyping of chromosomes prepared from the peripheral blood lymphocytes of a father of a child with mental retardation. The DAPI-banded (left) and the spectrally classified chromosomes (right) are shown. The fragment that was translocated to chromosome 1 could be identified as chromosome 11 material. This translocation was reciprocal because a small fragment that is derived from chromosome 1 was detected on the short arm of chromosome 11. The classification color for chromosome 1 is yellow, the one for chromosome 11 is blue (see Fig. 2). (**B**) High-resolution G-banding of metaphase chromosomes from a patient having ataxia. The banding pattern suggests chromosome 4 material translocated to chromosome 12. The classification unambiguously identified the additional material as being derived from chromosome 4. The translocation results in a partial trisomy of chromosome 4q. (**C**) DAPI staining of the marker chromosomes (mar1 through mar6) from the aneuploid breast cancer cell line SKBR3. The classification allows unambiguous characterization of even complex chromosomal aberrations, such as chromosomes containing homogeneously staining regions. The numbers indicate the origin of chromosomal material in the marker chromosomes. (**D**) Hybridization of chromosomes of the gibbon *Hylobates concolor* with painting probes for human chromosomes. The hybridization is presented in display colors, showing the intense staining of gibbon chromosomes with probes for human chromosomes. The numerous chromosomal rearrangements seen on the gibbon autosomes produce a multicolor banding pattern. (**E**) Classification-colored images of representative examples of gibbon chromosomes. The upper row presents examples of gibbon autosomes and the gibbon sex chromosomes that remain unchanged in the human karyotype. The center row shows gibbon chromosomes 5, 13, and 20 with whole-arm translocations from the human counterparts. Gibbon chromosomes 9, 19, and 22b (lower row) reveal multiple aberrations, producing a banding pattern. The numbers on the right side of the gibbon chromosomes indicate the corresponding human chromosome material.

REFERENCES AND NOTES

1. M. M. Le Beau, in *Important Advances in Oncology*, V. T. DeVita, S. Hellman, S. Rosenberg, Eds. (Lippincott, Philadelphia, 1993), pp. 29–45.
2. Z. Malik *et al.*, *J. Microscopy*, in press; Y. Garini *et al.*, in *Fluorescence Imaging Spectroscopy and Microscopy*, X. F. Wang and B. Herman, Eds. (Wiley, New York, 1996), vol. 137, pp. 87–124.
3. M. R. Speicher, S. G. Ballard, D. C. Ward, *Nature Genet.* **12**, 368 (1996).
4. Metaphase chromosomes from normal individuals, from patients with chromosomal abnormalities, and from tumor cell lines were prepared by standard methods. G-banding procedures followed standard protocols. We generated the chromosome painting probes by amplification of flow-sorted chromosomes with direct incorporation of fluorochrome-conjugated deoxyuridine 5′-triphosphate (dUTP) using degenerate oligonucleotide–primed polymerase chain reaction (DOP-PCR) [H. Telenius *et al.*, *Genes Chromosomes Cancer* **4**, 267 (1992)]. Five different fluorochrome-conjugated nucleotides (Cy2-dUTP, Spectrum Green–dUTP, Cy3-dUTP, Texas Red–dUTP, Cy5-dUTP) were used to label all 24 chromosomes (Amersham Life Science, Vysis, Molecular Probes). Combinatorial fluorescence was produced by combining differentially labeled chromosome painting probes. Hybridization and detection was essentially done as described [T. Ried, A. Baldini, T. C. Rand, D. C. Ward, *Proc. Natl. Acad. Sci. U.S.A.* **89**, 1388 (1992)]: 100 ng of each chromosome-specific library was ethanol precipitated in the presence of 10 μg of human Cot-1 DNA and resuspended in 10 μl of hybridization solution (50% formamide, 2× standard saline citrate, 10% dextran sulfate). After hybridization, the chromosome specimens were counterstained with 4′,6′-diamidino-2-phenylindole (DAPI), embedded in 1,4-diaza-

bicyclo[2.2.2] octane (DABCO)–glycerol and visualized on a Leica DMIRBE microscope equipped for epifluorescence. The DAPI banding was imaged with a cooled CCD camera (Photometrics, Tucson, AZ) or by spectral imaging through a DAPI-specific optical filter.

5. Spectral images were acquired and analyzed with the SD200 spectral bio-imaging system (Applied Spectral Imaging, Ltd., Migdal Haemek, Israel). The optical arrangement is schematically presented in Fig. 1. The SD200 imaging system attached to an inverted microscope (Leica DMIRBE) by means of a C-mount consists of an optical head with a special Fourier transform spectrometer (Sagnac common path interferometer) to measure the spectrum, and a cooled CCD camera (Princeton Instruments, Trenton, NJ) for imaging. The samples were illuminated with a Xenon lamp (OptiQuip 770/1600) and imaged with a 63× oil immersion objective through a custom-designed filter set (Chroma Technology, Brattleboro, VT) with broad emission bands (excitation filter: 486/28 nm, 565/16 nm, 642/22 nm; emission filter: 524/44 nm, 600/38 nm, 720/113 nm; beamsplitter: reflection 421 to 480 nm, 561 to 572 nm, 631 to 651 nm; transmission 495 to 564 nm, 580 to 620 nm, 660 to 740 nm). Excitation through this filter set allows all dyes to be excited and measured simultaneously without an image shift. The generation of a spectral image is achieved by acquiring ~100 frames of the same image. Each two frames differ only in the optical path differences (OPDs) created by a scanner controller in the interferometer. In this way the interferogram as the modulated function of intensity (that is, the intensity as a function of OPD) is measured simultaneously for each pixel in the image. However, each pixel functions like a stand-alone Fourier transform spectrometer. Measurement times vary depending on the brightness and the size of the image, the desired spectral resolution, and the signal-to-noise ratio. A typical measurement for chromosome painting probes takes about 50 s with a 15-nm (at 600 nm) spectral resolution. The spatial resolution of the measurement is ~0.24 μm and is limited by the CCD pixel size (15 μm) and the objective magnification (63×). After the measurement, ~2 min are required to build the spectral image with a software-based fast Fourier transform (FFT) algorithm [E. O. Brigham, *The Fast Fourier Transform and its Application* (Prentice-Hall, Englewood Cliffs, NJ, 1988)]. The conversion of emission spectra to visualize the spectral image in display colors is achieved as follows: The measured spectrum at each pixel is divided into three spectral ranges (475 to 550 nm, 550 to 650 nm, and 650 to 750 nm). Each of the spectral ranges is visualized in a different color (blue, green, and red, respectively). The intensity for each color is proportional to the integrated intensity in the corresponding spectral range (Figs. 1 and 2).
6. One of the most important analysis algorithms is the spectral-based classification algorithm that enables multiple different spectra in the image to be identified and highlighted in classification colors. This allows assignment of a specific classification color to all human chromosomes on the basis of their spectra. This algorithm assumes that the (reference) spectrum of each chromosome has been measured and stored in a reference library in the computer. A classification color is assigned to each pixel in the image according to the classification color assigned to the reference spectrum that is most similar to the spectrum at the given pixel. A minimal square error algorithm $S_{x,y,n} = \Sigma\,[I_{x,y}(\lambda) - I_n(\lambda)]^2$ is computed for every pixel, in which $I_{x,y}(\lambda)$ is the normalized spectrum at pixel coordinates x,y, and $I_n(\lambda)$ represents the normalized reference spectrum for each of the chromosome $n = 1, 2, \ldots 23$ (X), 24 (Y). After calculating the value of $S_{x,y,n}$ for all reference spectra, the smallest value is chosen and a classification color is assigned to that pixel in accordance with the classification color assigned to the most similar reference spectrum.
7. Y. Ning, *Nature Genet.*, in press.
8. E. Schröck *et al.*, unpublished data.
9. A. Kallioniemi *et al.*, *Proc. Natl. Acad. Sci. U.S.A.* **91**, 2156 (1994).
10. U. Koehler, F. Bigoni, J. Wienberg, R. Stanyon, *Genomics* **30**, 287 (1995); P. van Tuinen and D. H. Ledbetter, *Am. J. Phys. Anthropol.* **61**, 453 (1983).
11. P. Meltzer, X.-Y. Guan, A. Burgess, J. Trent, *Nature Genet.* **1**, 2 (1992).

12. E.S. received a stipend from the Deutsche Forschungsgemeinschaft. I.B. is a postdoctorate student in S. Lavi's lab. We would like to thank P. Millman (Chroma Technology) and A. Waggoner (Amersham Life Sciences) for valuable discussions, and D. Leja for help in preparing Fig. 1. T. Knutsen, K. Precht, M. Macha, the cytogenetics laboratory of American Medical Laboratories, and Children's Hospital, Chantilly, VA, kindly provided metaphase chromosome preparations. The continued support of R. Buckwald, D. Cabib, N. Katzir, D. Wine, and M. Lavi (Applied Spectral Imaging, Ltd.) is gratefully acknowledged. We are indebted to J. Trent and M. Bittner for critically reading the manuscript.

23 January 1996; accepted 20 May 1996

Control Strategies for Tuberculosis Epidemics: New Models for Old Problems

S. M. Blower,* P. M. Small, P. C. Hopewell

Tuberculosis, although preventable and curable, causes more adult deaths than any other infectious disease. A theoretical framework for designing effective control strategies is developed and used to determine treatment levels for eradication, to assess the effects of noneradicating control, and to examine the global goals of the World Health Organization. The theory is extended to assess how suboptimal control programs contribute to the evolution of drug resistance. A new evaluation criterion is defined and used to suggest how control strategies can be improved. In order to control tuberculosis, treatment failure rates must be lower in developing countries than in developed countries.

For many years tuberculosis has been both a preventable and a curable disease. Isoniazid is used to prevent individuals latently infected with *Mycobacterium tuberculosis* from developing disease, and regimens consisting of multiple drugs are highly successful in curing active cases (*1*). However, tuberculosis still causes more adult deaths worldwide than any other infectious disease (*2*). This finding suggests that many of the current control strategies that have been empirically designed are in need of improvement; recent increases in cases caused by drug-resistant organisms, many of which have arisen as a result of treatment failure, have exacerbated the control problems (*3*). We suggest that new control strategies can be designed based on a quantitative understanding of the transmission dynamics of tuberculosis.

In previous studies, we formulated and analyzed mathematical models that enable understanding of the intrinsic transmission dynamics of untreated tuberculosis epidemics and interpretation of the historical epidemiology of this disease (*4*–*6*). These transmission models reflect current biomedical understanding of the pathogenesis of tuberculosis. We have extended these models to include the population level effects of chemoprophylaxis and treatment (*7*); using this chemoprophylaxis and treatment model (Fig. 1), we have developed a theoretical framework for designing effective tuberculosis control strategies (*8*).

We assessed the epidemic control effects of treatment and chemoprophylaxis by deriving the effective reproductive rate (R) of tuberculosis from our model

$$R = \left(\frac{\beta\Pi}{\mu}\right)\left(\frac{1}{\phi + \mu + \mu_T}\right)\left(p + \frac{(1-p)\nu}{\sigma + \nu + \mu}\right) \quad (1)$$

where β is the transmission coefficient for tuberculosis; the other parameters are defined in (*7*).

R is the average number of secondary infectious cases that are produced when one infectious case is introduced into a disease-free population in which a program of chemoprophylaxis or treatment (or both) is in place (*9*). Consequently, R is an epidemiological measure of the severity of an epidemic; if $R > 1$, an epidemic may occur, but if $R < 1$, an epidemic will die out.

The value of R is determined by the product of three components (Eq. 1): the effective contact rate {defined as the average number of susceptibles that one infectious case infects per unit time $[(\beta\Pi)/\mu]$}, the average duration of infectiousness of a case $[1/(\phi + \mu + \mu_T)]$, and the probability that an infected individual will become an infectious case {defined as p for primary progressive and $[(1 - p)\nu]/(\sigma + \nu + \mu)$ for reactivation tuberculosis}. Equation 1 can be used to qualitatively and quantitatively assess the effects of chemoprophylaxis and treatment for epidemic control. Qualitatively, an increase in the chemopro-

S. M. Blower, Department of Epidemiology and Biostatistics and Department of Medicine, University of California, San Francisco, Box 1347, San Francisco General Hospital, San Francisco, CA 94143–1347, USA.
P. M. Small, Department of Medicine, Stanford Medical School, Stanford, CA 94305, USA.
P. C. Hopewell, Department of Medicine, University of California, San Francisco, San Francisco General Hospital, San Francisco, CA 94143–1347, USA.

*To whom correspondence should be addressed. E-mail: sally@cygnus.ucsf.edu

Multicolor Spectral Karyotyping of Human Chromosomes

E. Schröck, S. du Manoir, T. Veldman, B. Schoell, J. Wienberg, M. A. Ferguson-Smith, Y. Ning, D. H. Ledbetter, I. Bar-Am, D. Soenksen, Y. Garini and T. Ried

Science **273** (5274), 494-497.
DOI: 10.1126/science.273.5274.494